Analysis and design of fibers for pure-quartic solitons

Lo, Chih-Wei; Stefani, Alessio ; de Sterke, C. Martijn; Blanco-Redondo, A.

Published in:
Optics Express

Link to article, DOI:
10.1364/OE.26.007786

Publication date:
2018

Document Version
Publisher's PDF, also known as Version of record

Research Article | Vol. 26, No. 6 | 19 Mar 2018 | OPTICS EXPRESS 7786
Optics EXPRESS

Analysis and design of fibers for pure-quartic solitons

CHIH-WEI LO,[1,2] A. STEFANI,[2,3] C. MARTIJN DE STERKE,[1,2] AND A. BLANCO-REDONDO[1,2,4*]

[1]*Centre for Ultrahigh-bandwidth Devices for Optical Systems (CUDOS), School of Physics, University of Sydney 2006, Australia*
[2]*Institute of Photonics and Optical Science, School of Physics, University of Sydney 2006, Australia*
[3]*DTU Fotonik, Department of Photonics Engineering, Technical University of Denmark, DK-2800, Kgs. Lyngby, Denmark*
[4]*The University of Sydney Nano Institute (Sydney Nano), Sydney Nanoscience Hub, University of Sydney 2006, Australia*
[*]*andrea.blancoredondo@sydney.edu.au*

Abstract: The recently discovered pure-quartic solitons, arising from the interaction of quartic dispersion and Kerr nonlinearity, open the door to unexplored soliton regimes and ultrafast laser science. Here, we report a general analysis of the dispersion and nonlinear properties necessary to observe pure-quartic solitons in optical platforms. We apply this analysis, in combination with numerical calculations, to the design of pure-quartic soliton supporting microstructured optical fibers. The designs presented here, which have realistic fabrication tolerances, support unperturbed pure-quartic soliton propagation providing access to an unmatched platform to study novel soliton physics.

OCIS codes: (190.5530) Pulse propagation and temporal solitons; (060.4005) Microstructured fibers; (060.4370) Nonlinear optics, fibers.

References and links

1. A. Blanco-Redondo, C. M. de Sterke, J. E. Sipe, T. F. Krauss, B. J. Eggleton, and C. Husko, "Pure-quartic solitons," Nat. Commun. **7**, 10427 (2016).
2. V. E. Zakharov and A. B. Shabat, "Exact theory of two-dimensional self-focusing and one-dimensional self-modulation of waves in nonlinear media," Sov. Phys. JETP **34**(1), 62-69 (1972).
3. A. Hasegawa, and F. Tappert, "Transmission of stationary nonlinear optical physics in dispersive dielectric fibers. I. anomalous dispersion," Appl. Phys. Lett. **23**, 142-144 (1973).
4. Y. S. Kivshar and G. P. Agrawal, *Optical Solitons: From Fibers to Photonic Crystals* (Academic, 2003).
5. G. P. Agrawal, *Nonlinear Fiber Optics, Fifth Edition* (Academic, 2013).
6. A. Blanco-Redondo, C. Husko, D. E. Eades, Y. Zhang, J. Li, and T. F. Krauss, "Observation of soliton compression in silicon photonic crystal waveguides," Nat. Commun. **5**, 3160 (2014).
7. I. Christov, M. N. Murnane, H. C. Kapteyn, J. Zhou, and C.-P. Huang, "Fourth-order dispersion-limited solitary pulses," Opt. Lett. **19**(18), 1465-1467 (1994).
8. K. J. Blow, N. J. Doran, and D. Wood, "Generation and stabilization of short soliton pulses in the amplified nonlinear Schrödinger equation," J. Opt. Soc. Am. B **5**(2), 381-389 (1988).
9. A. Höök and M. Karlsson, "Ultrashort solitons at the minimum-dispersion wavelength: effects of fourth-order dispersion," Opt. Lett. **18**(17), 1388-1390 (1993).
10. M. Karlsson and A. Höök,"Soliton-like pulses governed by fourth-order dispersion in optical fibers," Opt. Commun. **104**(4-6), 303-307 (1994).
11. N. Akhmediev,A. V. Buryak, and M. Karlsson, "Radiationless optical solitons with oscillating tails," Opt. Commun. **110**(5-6), 540-544 (1994).
12. M. Piché, J.-F Cormier, and X. Zhu, "Bright optical soliton in the presence of fourth-order dispersion," Opt. Lett. **21**(12), 845-847 (1996).
13. V. E. Zakharov and E. A. Kuznetsov, "Optical solitons and quasisolitons," J. Exp. Theor. Phys. **86**(5), 1035-1045 (1998).
14. S. Roy and F. Biancalana, "Formation of quartic solitons and a localized continuum in silicon-based waveguides," Phys. Rev. A **87**, 025801 (2013).
15. P. Colman, C. Husko, S. Combrie, I. Sagnes, C. W. Wong, and A. De Rossi, "Temporal solitons and pulse compression in photonic crystal waveguides," Nat. Photonics **4**, 862-868 (2010).

#320010 https://doi.org/10.1364/OE.26.007786
Journal © 2018 Received 18 Jan 2018; revised 6 Mar 2018; accepted 7 Mar 2018; published 16 Mar 2018

Optics EXPRESS

16. K. J. A. Ooi, D. K. T. Ng, T. Wang, A. K. L. Chee, S. K. Ng, Q. Wang, L. K. Ang, A. M. Agarwal, and D. T. H. Tan, "Pushing the limits of CMOS optical parametric amplifiers with USRN: Si_7N_3 above the two-photon absorption edge," Nat. Commun. **8**, 13878 (2017).
17. L. Yin, and G. P. Agrawal, "Impact of two-photon absorption on self-phase modulation in silicon waveguides," Opt. Lett. **32**(14), 2031-2033 (2007).
18. A. Blanco-Redondo, D. Eades, J. Li, S. Lefrancois, T. F. Krauss, B. J Eggleton, and C. Husko, "Controlling free-carrier temporal effects in silicon by dispersion engineering," Optica **1**(5), 299-306 (2014).
19. S. Lefrancois, C. Husko, A. Blanco-Redondo, and B. J Eggleton, "Nonlinear silicon photonics analized with the moments method ," J. Opt. Soc. Am. B **32**(2), 218-226 (2015).
20. T. P. White, R. C. McPhedran, C. M. de Sterke, L. C. Botten, and M. J. Steel, "Confinement losses in microstructured optical fibers," Opt. Lett. **26**(21), 1660-1662 (2001).
21. P. Russell, "Photonic crystal fibers," Science, **299**, 358-362 (2003).
22. T. M. Monro, D. J. Richardson, N. G. R. Broderick and P. J. Bennett,"Holey optical fibers: an efficient modal model," J. Lightwave Technol. **17**(6), 1093-1102, (1999).
23. M.J. Gander, R. McBride, J. D. C. Jones, D. Mogilevtsev, T. A. Birks, J. C. Knight, and P. St. J. Russell, "Experimental measurement of group velocity dispersion in photonic crystal fibre," Electron. Lett. **35**(1), 63-64, (1999).
24. J. C. Knight, J. Arriaga, T. A. Birks, A. Ortigosa-Blanch, W. J. Wadsworth, and P. St. J. Russell,"Anomalous dispersion dispersion in photonic crystal fiber," IEEE Photonics Technol. Lett. **12**, 807-809, (2000).
25. A. Ferrando, E. Silvestre, J. J. Miret, and P. Andrés,"Nearly zero ultraflattened dispersion in photonic crystal fibers," Opt. Lett. **25**(11), 790-792, (2000).
26. F. Poletti, V. Finazzi, T. M. Monro, N. G. R. Broderick, V. Tse, and D. J. Richardson,"Inverse design and fabrication tolerances of ultra-flattened dispersion holey fibers," Opt. Express **13**(10), 3728-3736, (2005).
27. D. J. J. Hu, P. P. Shum, C. Lu, and G. Ren,"Dispersion-flattened polarization-maintaining photonic crystal fiber for nonlinear applications," Opt. Commun. **282**(20), 4072-4076, (2009).
28. H. Xu, J. Wu, K. Xu, Y. Dai, C. Xu, and J. Lin,"Ultra-flattened chromatic dispersion control for circular photonic crystal fibers," J. Opt. A, Pure Appl. Opt. **13**(5), 055405 (2011).
29. A. Ferrando, E. Silvestre, P. Andres, J. Miret, and M. Andres, "Designing the properties of dispersion-flattened photonic crystal fibers,âĂİ Opt. Express **9**(13), 687-697 (2001).
30. W. Reeves, J. Knight, P. Russell, and P. Roberts, "Demonstration of ultra-flattened dispersion in photonic crystal fibers," Opt. Express **10**(14), 609-613 (2002).
31. S. P. Stark, F. Biancalana, A. Podlipensky, and P. St. J.Russell, "Nonlinear wavelength conversion in photonic crystal fibers with three zero-dispersion points," Phys. Rev. A - At. Mol. Opt. Phys. **83**(2), 1-5 (2011).
32. K. Saitoh, M. Koshiba, T. Hasegawa, and E. Sasaoka, "Chromatic dispersion control in photonic crystal fibers: application to ultra-flattened dispersion," Opt. Express **11**(8), 843-852 (2003).
33. B. Kuhlmey, G. Renversez, and D. Maystre, "Chromatic dispersion and losses of microstructured optical fibers," Appl. Opt., **42**(4), 634-639 (2003).
34. sydney.edu.au/science/physics/cudos/research/mofsoftware.shtml
35. T. P. White, B. T. Kuhlmey, R. C. McPhedran, D. Maystre, G. Renversez, C. M. de Sterke, and L. C. Botten, "Multipole method for microstructured optical fibers. I. Formulation," J. Opt. Soc. Am. B , **19**, 2322-2330 (2002).
36. B. T. Kuhlmey, T. P. White, C. M. de Sterke, D. Maystre, G. Renversez, R. C. McPhedran, and L. C. Botten, "Multipole method for microstructured optical fibers II: Implementation and results," J. Opt. Soc. Am. B , **19**(10), 2331-2340 (2002).
37. A. Stefani, M. H. Frosz, T. G. Euser, G. K. L. Wong, and P. St. J. Russell, "Real-time Doppler-assisted tomography of microstructured fibers by side-scattering," Opt. Express **22**(21), 25570-25579 (2014).
38. S. R. Sandoghchi, G. T. Jasion, N. V. Wheeler, S. Jain, Z. Lian, J. P. Wooler, R. P. Boardman, N. Baddela, Y. Chen, J. Hayes, E. Numkam Fokoua, T. Bradley, D. R. Gray, S. M. Mousavi, M. Petrovich, F. Poletti, and D. J. Richardson, "X-ray tomography for structural analysis of microstructured and multimaterial optical fibers and preforms," Opt. Express **22**(21), 26181-26192 (2014).

1. Introduction

Pure-quartic solitons (PQSs) are a novel class of solitary optical waves that arise from the interaction of negative fourth-order dispersion (FOD) and self-phase modulation (SPM) [1]. Due to the Kerr nonlinearity of the medium, intense optical pulses undergo SPM, which generates new red (blue) frequencies at the trailing (leading) edge of the pulse. In the presence of negative FOD the red frequencies travel faster than the blue frequencies, which compensates the effect of SPM and keeps the pulse from spreading either in time or in frequency. This soliton formation mechanism, which is analogous to that of conventional nonlinear Schrödinger (NLS) solitons [2–6], can in principle be extended to all the even orders of dispersion.

The idea that soliton-like behavior could arise from the interplay of negative FOD and SPM

Optics EXPRESS

was suggested in the early 90's by Christov et al. [7], in the context of a Ti:sapphire laser system operating at near-zero group-velocity dispersion (GVD) and third-order dispersion (TOD). Other theoretical efforts aimed to elucidate the behavior of NLS solitons in the presence of significant FOD [8–14]. Given the difficulty of engineering optical platforms with dominant FOD over a sufficiently large bandwidth, most of these predictions were never experimentally confirmed. Recently, however, some of us demonstrated experimentally the existence of PQSs in a dispersion-engineered slow-light silicon photonic crystal waveguide (PhC-wg) [1]. In this nanophotonic platform, the FOD effect was strongly dominant over all the other orders of dispersion at wavelengths centered around $\lambda_0 = 1550$ nm and for pulse durations $T_0 \approx 0.8$ ps, across a bandwidth of approximately $4 - 5$ nm. This strong FOD was balanced by the slow-light enhanced SPM in the silicon PhC-wg giving rise to PQSs in a few hundred microns waveguide. Although the advantages of this particular nanophotonic platform are numerous – CMOS compatibility, compact footprint, low power required – it is crucial to extend the demonstration of PQSs to other physical platforms to prove that they are a general optical phenomenon and to extend their application range.

PQSs are interesting in their own right. Aside from their different physical origin, PQSs present significant differences with respect to every other soliton reported to date. For instance, they can occur with normal or zero GVD, expanding the available wavelength range for soliton functionality in optical media; the PQS shape [1] is different to that of conventional NLS solitons or any other optical soliton observed to date [4]; more importantly, perhaps, one of the key features of PQSs is their advantageous energy scaling, $U \propto T_0^{-3}$, with respect to NLS solitons, $U \propto T_0^{-1}$. This yields dramatically higher PQS energies at low pulse durations creating an outstanding potential for ultrafast lasers and opening up new avenues of study for supercontinuum generation and frequency combs. Nanophotonics platforms, however, are inherently confined to sub-nanojoule energies [15, 16] and therefore not suitable to exploit this advantage. Further, the PQSs measurements in Ref. [1], were strongly perturbed by the effect of the two-photon absorption (TPA) generated free-carriers in silicon, namely asymmetrical blue-shift and self-acceleration of the pulse [17–19].

In contrast to nanophotonic platforms, silica microstructured optical fibers (MOFs) [20, 21] are TPA-free and can support very high energies while still providing excellent possibilities for dispersion engineering. MOFs guide light by a modified form of total internal reflection in a solid core, generally silica, surrounded by a cladding of air holes. The strong index contrast between core and cladding gives rise to tight optical confinement, which enhances the nonlinearities, and a strongly wavelength-dependent effective index that can overcome material dispersion [22]. These remarkable dispersion-engineering possibilities have enabled fine tuning of the zero-dispersion wavelength (ZDW) in a broad spectral range [23, 24] and even the realization of dispersion profiles with three [25, 26] and four ZDWs [27, 28].

Here, by using dispersion-engineering, we present a design approach and final realizable designs for MOFs with dominant negative quartic dispersion that can support PQS propagation. We start by discussing the dispersion requirements necessary to achieve PQS propagation, followed by a brief discussion on the desirable nonlinear properties. Next we provide a detailed approach to design MOF fibers fulfilling those requirements and complying with the fabrication constraints. Finally we study a realizable designs in detail and characterize its performance for PQS propagation by providing nonlinear Schrödinger equation (NLSE) simulations.

2. Dispersion requirements

The observation of PQSs requires that the quartic dispersion is negative, that it dominates for the pulse durations of interest, and that the nonlinear coefficient is sufficiently large so the nonlinearity can balance the quartic dispersion for practical values of the peak power. In practice, the requirements on the dispersion are much more difficult to meet and we examine them first.

Optics EXPRESS

We consider a dispersive waveguide and neglect all dispersion of fifth order and higher, so that $\beta_2 = \beta_2(\omega)$ is a quadratic function of frequency. A necessary condition for the observation of PQSs is that $\beta_4 < 0$. Without loss of generality, we can then define frequency ω_0 such that $\beta_3(\omega_0) \equiv \partial\beta_2/\partial\omega|_{\omega=\omega_0} = 0$, and can thus write the relationship between the group velocity dispersion β_2 and the frequency ω as

$$\beta_2(\omega) = \beta_{20} - \frac{1}{2}|\beta_{40}|\,(\omega - \omega_0)^2\,. \tag{1}$$

Thus $\beta_2 = \beta_{20}$ at ω_0 and varies quadratically at other frequencies with a curvature given by $\beta_{40} < 0$; if $\beta_{20} > 0$ then $\beta_2 = 0$ when $\omega = \omega_0 \pm \sqrt{2\beta_{20}/|\beta_{40}|} \equiv \omega_0 \pm \delta\omega$.

To estimate the influence of the various dispersion orders, following Agrawal [5], we introduce the dispersion lengths $L_p = T_0^p/|\beta_p|$, with p representing the dispersion order. Ideally, the dispersion of our waveguide is such that for a suitable pulse duration, $L_4 \ll L_{2,3}$. For the dispersion relation in Eq. (1) we find that

$$L_2 = \frac{T_0^2}{|\beta_{20} - \frac{1}{2}|\beta_{40}|\,(\omega-\omega_0)^2\,|}, \qquad L_3 = \frac{T_0^3}{|\beta_{40}\,(\omega-\omega_0)\,|}, \qquad L_4 = \frac{T_0^4}{|\beta_{40}|}. \tag{2}$$

Their frequency dependence is schematically shown in Fig. 1(a). Here and below we take $\beta_{20} > 0$ as will be justified later. Thus L_2 (dashed-dotted red) diverges at $\omega - \omega_0 = \pm\delta\omega$, whereas L_3 (dashed blue) diverges at $\omega - \omega_0 = 0$. In this approximation L_4 (solid black) does not depend on frequency. While Fig. 1(a) refers to a particular pulse duration T_0, the pulse duration-dependence follows from Eqs. (2). Thus shortening the pulse strengthens the effect of higher-order dispersion (and thus shortens L_4 w.r.t. L_3, and L_3 w.r.t. L_2).

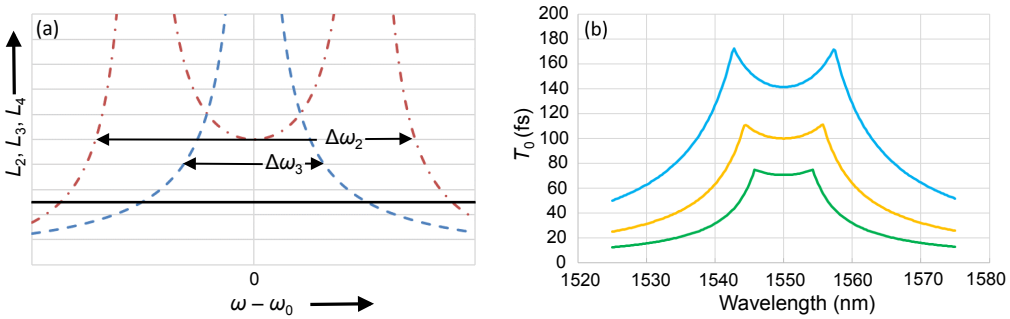

Fig. 1. (a) Schematic of the characteristic lengths L_2 (dashed-dotted red), L_3 (dashed-blue), and L_4 (solid black), versus frequency for $\beta_{20} > 0$. The frequency regions $\Delta\omega_2$ and $\Delta\omega_3$ are indicated for $\alpha_2 = 2$ and $\alpha_3 = 1.6$; (b) Pulse duration as a function of wavelength for which the conditions in Eq. (3) are met for $\alpha_2 = \alpha_3 = 1$ (blue curve), $\alpha_2 = \alpha_3 = 2$ (yellow curve) $\alpha_2 = \alpha_3 = 4$ (green curve).

While shortening the pulses increases the effect of β_4, it also broadens the bandwidth over which it needs to dominate. To investigate this further we quantify the degree to which the quartic dispersion needs to dominate the lower order dispersion for a PQS to exist through

$$L_2 \geq \alpha_2 L_4, \qquad L_3 \geq \alpha_3 L_4, \tag{3}$$

where $\alpha_{2,3} > 1$. Considering Fig. 1(a) we note that the first of Eqs. (3) needs to be satisfied at ω_0. This immediately leads to the requirement

$$\frac{|\beta_{40}|}{\beta_{20}} \geq \alpha_2 T_0^2 \tag{4}$$

Optics EXPRESS

The bandwidth over which this condition is satisfied can be found from the frequency for which the denominator of the first of Eqs. (2) changes sign with respect to $\omega = \omega_0$ (see Fig. 1(a)), so

$$\Delta\omega_2 = 4\sqrt{\frac{\beta_{20}}{|\beta_{40}|}}, \tag{5}$$

which does not depend on α_2. Similarly, the second of Eqs. (3) leads to

$$\Delta\omega_3 \leq \frac{2}{\alpha_3 T_0}. \tag{6}$$

We can express these results in terms of time-bandwidth products of the pulse duration and the spectral widths for which Eqs. (3) are satisfied, namely

$$\Delta\omega_3 T_0 \leq \frac{2}{\alpha_3}, \qquad \Delta\omega_2 T_0 \leq \frac{4}{\sqrt{\alpha_2}}. \tag{7}$$

Since $\alpha_{2,3} > 1$, we find that the first of these is the most restrictive, consistent with Fig. 1(a). Since the time-(angular) bandwidth product for a Gaussian and for hyperbolic secant pulses is $2\pi \times 0.44 \approx 2.8$ and $2\pi \times 0.32 \approx 2.0$, we conclude that in the approximation, in which we neglect 5th and higher order dispersion, it is possible for the 4th order dispersion to dominate over a substantial fraction of the pulse spectrum. However, a more detailed statement requires knowledge of shape of PQSs and of parameter α_3.

An alternative way to represent the information is shown in Fig. 1(b). It shows the pulse durations for which the two conditions in Eq. (3) are satisfied for $\alpha_2 = \alpha_3 = 1$ (blue curve), $\alpha_2 = \alpha_3 = 2$ (yellow curve), and $\alpha_2 = \alpha_3 = 4$ (blue curve). Consistent with Fig. 1(a), the part of the curves closest to $\lambda_0 = 1550$ nm are determined by β_2, while the sections further away are determined by β_3. Figure 1(b) confirms that the available bandwidth decreases when the values of $\alpha_{2,3}$ increase.

3. Fiber design method

Once the dispersion requirements are understood, the question is whether we can meet them in fiber platforms. In contrast to the material dispersion of silica, which has a large and monotonically decreasing negative β_2 and large positive β_3 around 1550 nm, the PQS-supporting fiber must have $\beta_2, \beta_3 \approx 0$ and $\beta_4 < 0$ over a sufficiently wide bandwidth around that center wavelength. Fibers with such a dispersion profile have been reported in the context of three ZDWs and ultra-flattened dispersion MOFs. Two approaches have led to similar dispersion curves, each with advantages and disadvantages. The first approach is to use a uniform array of holes [25, 29–31]. This type of MOF is simple to fabricate, as the applied pressure can be kept constant throughout the structure. However, to obtain the desired dispersion profile described in Eq. (1) with uniform holes, the hole size (d) and the hole-to-pitch ratio (d/Λ) have to be small: $d \approx 600$ nm and $d/\Lambda \approx 0.24 - 0.3$. Such fiber parameters lead to large confinement loss which can only be compensated by a huge number of rings of holes, which strongly complicates the fabrication. The second approach is to use rings of holes with a gradient in hole size, *i.e.*, each ring of holes is composed of holes of the same size, but the hole size increases for rings further away from the center of the fiber [26, 32]. These structures allow for excellent control of the dispersion, and allow us to achieve the desired profile. However, they require a different applied pressure to each ring to achieve the desired hole area and to maintain the holes from collapsing because of surface tension. Having differential pressures for each hole size is hard to realize at the cane level and, although allowing for great fabrication flexibility, it introduces a large number of parameters that can be changed independently and makes the process hard to fully exploit. Probably because of

Optics EXPRESS

the complications related to the fabrication, to the best of our knowledge, no fibers with graded holes have been fabricated with similar dispersion profiles to the desired one. It should be noted that in all proposed designs the hole-to-hole distance (or pitch, Λ) is constant across the entire fiber because the capillaries used for stacking are required to have the same size in order to obtain an hexagonally packed structure.

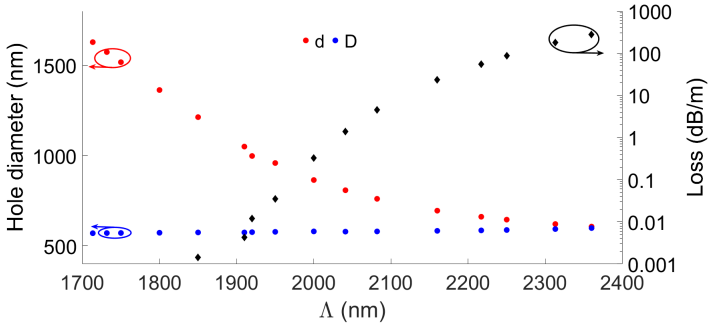

Fig. 2. Hole sizes (d in blue and D in red) for various hole spacing (Λ) of the simulated structures with dominant FOD and with zero of TOD centered at 1550 nm. The black diamonds represent the simuated loss corresponding to those structures.

We find a compromise that combines the advantages of the two approaches mentioned above. Thus, we design a fiber structure that provides the desired dispersion while meeting the fabrication constraints. To this purpose, we limit the number of rings to a maximum of 5 and with just 2 different hole sizes. The innermost holes are small and have a strong impact on the dispersion, while the outermost holes are larger and act as a barrier to reduce confinement loss. We also aim to find structures with dominant FOD close to λ_0 = 1550 nm (corresponding to ω_0 in Eq (1) and Fig. 1). The parameters to investigate are the number of rings with small holes and large holes, the pitch of the structure Λ, the diameter of the small holes d, and the diameter of the large holes D. As discussed below, we choose to use all 5 rings of holes and to have more holes with larger holes than with small ones, in particular 3 and 2. From previous investigations [26, 29, 33] it is known that the pitch of the structure determines the position of ω_0. Values of Λ between 1.5 and 2.7 μm have been proposed for dispersion curves with the required trend.

We started our investigation from fiber F3 of Ref. [26]. We optimized the number of rings with large and small holes and fine tuned the structure to achieve the desired dispersion profile, keeping in mind the fabrication constraints. We also look into structures for which β_{20} >0 , in order to prevent the competition of ordinary and pure quartic solitons, leading to three-zero-dispersion curves. Moreover, we initially considered $\alpha_3 = \alpha_2 = 1$ for simplicity, requiring the FOD to be the dominant dispersion term.

We performed numerical simulations by using the CUDOS Microstructured Optical Fiber (MOF) solver [34], which uses the multipole method to calculate the effective index [35, 36].

After few preliminary simulations, we realized that having a larger number of rings with large holes makes it easier to move the dispersion curve across wavelengths and still keep the desired curvature. However, it also made the dispersion more sensitive to small changes in the design parameters. Also, a large number of rings with large holes improved the confinement with a smaller difference between the size of the large and small holes. In order to compromise between wavelength and guidance, we chose the above mentioned combination of 2 rings of small holes and 3 rings of large holes.

With this structure we changed the pitch and adjusted the size of small and large holes to obtain structures that still had a FOD dominant region around 1550 nm but trying to obtain as close size

Optics EXPRESS

as possible between the small and the large holes. Figure 2 shows the parameters for some of the structures. It is clear that the size of the small holes (around 600 nm) is the dominant factor and it changes very little. This is in agreement with the structures of both Ref. [31] and [26]. In approaching the ideal condition for fiber drawing, which is uniform holes, the pitch has to become larger and the structure approaches the the one from Ref. [31] and fiber F4 of Ref. [26]. As already mentioned, at this stage the loss become a crucial factor. The black diamonds in Fig. 2 show the loss for the simulated structures.

3.1. Fine tuning and robustness

Once we identified the parameters of interest we look at how small variations of the structure influence the dispersion in order to both be able to fine tune the dispersion profile and to estimate its robustness to fabrication tolerances. For this purpose we selected one of the structures from Fig. 2 (particularly the one with $\Lambda = 1.92$ μm as will become clear below) and changed the three parameters (d,D,Λ) independently by 1% both in the positive and the negative direction. The resulting β_2, β_3 and β_4 curves are shown in Figs. 3(a)- 3(i).

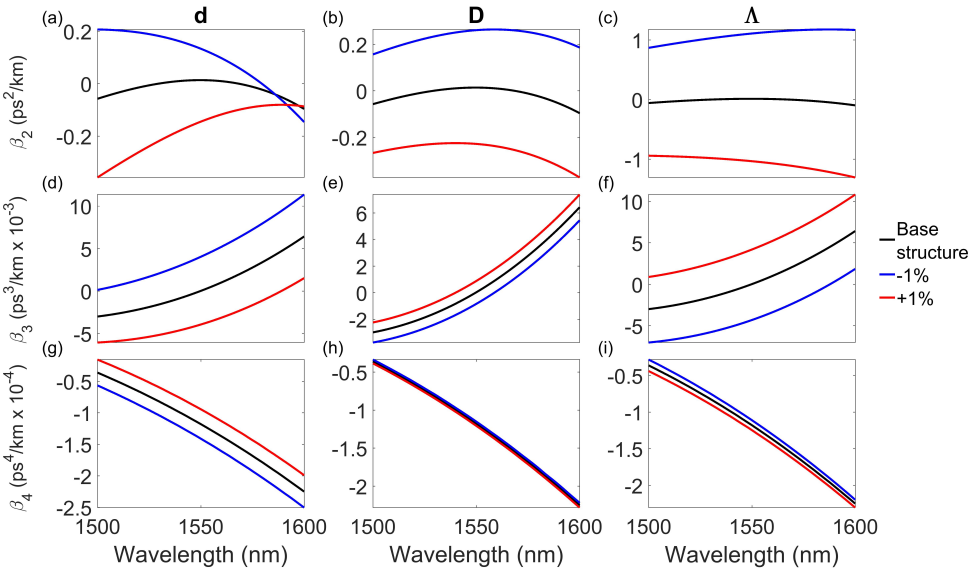

Fig. 3. β_2 (a-c), β_3 (d-f), and β_4 (g-i) curves for fiber structures with ±1% variations in d (a,d,g), D (b,e,h) and Λ (c,f,i) from a selected structure. The black curve represent the base structure, while the blue and the red curve represent the case for which the specific parameter is 1% smaller and larger than the base structure, respectively.

It becomes immediately clear that changing the various parameters has a noticeably larger effect on β_2 than on β_4. The advantage here is two-fold: we can tune the structure by focusing primarily on β_2, which is simpler than having to work with higher orders of dispersion; and, given that β_4 remains negative and largely unchanged against small changes, all these structures should be able to support PQS propagation even in the presence of fabrication tolerances. The effect on β_3 is effectively a shift of the zero-TOD wavelength, which can be addressed by tuning the operational wavelength.

We now have a closer look to the effect of the various parameters. Small increase (decrease) in the size of d leads to a combined effect of shifting the β_2 curve to lower (higher) values and to longer (shorter) wavelengths, as shown in Fig. 3(a). Moreover, as it becomes apparent in Fig. 3(g), small changes to the small holes size have the largest impact on β_4. This is not surprising as the

Optics EXPRESS

inner holes have a larger interaction with the guided mode. Also, it is consistent with the results in Fig. 2, where almost constant d was necessary to keep the maximum of β_2 close to 1550 nm. It is also worth noticing that a 1% change in d is smaller in absolute value compared to the other parameters. Modifications of both D – Figs. 3(b), 3(e), and 3(h) – and Λ – Fig. 3(c), 3(f), and 3(i) – show similar effects on β_2, β_3 and β_4, with the effect of changing Λ being larger in magnitude (even when considered the change in absolute value). This explains why a decrease of D was necessary when increasing Λ (Fig. 2) in order to keep β_2 just above zero while keeping λ_0 fixed. Given this analysis, the easiest way to fine-tune the dispersion is by small changes in D. However, this is not easy from a fabrication point of view.

During fiber fabrication, the parameter on which there is the most control is the holes spacing Λ. In fact, the outer size of the fiber is constantly monitored during drawing and the spacing between the holes is fixed to the outer diameter by preparation of the preform. Instead, the diameter of the holes is not known in real time and it depends on both the applied pressure and the tension (which is related to the drawing temperature and velocities). Despite some techniques having been investigated for monitoring the structure of highly scattering fibers [37, 38] none is currently used in fiber fabrication. Therefore, adjusting Λ is a more reliable way to tune the dispersion. However, it should be remembered that changing the size of the fiber also changes the size of the holes.

The fiber fabrication process, although very well developed, is not expected to yield perfect matching with the design. Further, the structural parameters may not be perfectly constant along the fiber length. In this investigation, we consider the latter to be of minor importance, since the required lengths are on the order of a few meters. Moreover, in practice, random variations in the holes sizes can also be expected. However, a proper characterization of the effect of randomness is a computationally hard task. Instead, a linear combination of the presented effects can be used as a reasonable approximation to random variations. From Fig. 3 we can infer the robustness of the dispersion to fabrication deviations from the design. As mentioned, β_4 stays negative and quite unchanged for reasonable variations of all the parameters. Therefore, the ability of the structure to support PQS depends on whether or not the FOD dominates. Even if Fig. 3 shows relatively large changes in the value of β_2, it should be emphasized from Eq. (4) that shortening the pulse compensates quadratically for a change in ratios between β_4 and β_2. This provide us with a useful control knob, the pulse duration, to achieve PQS propagation even in non-ideal structures.

4. Pure-quartic soliton supporting fiber

We now focus our attention in a particular MOF design and demonstrate that, consistent with the analytic results from Section 2, it can support the propagation of PQSs using numerical solutions of the generalized NLSE [1].

In order to choose the most promising MOF design from the plethora of results presented in Fig. 2, we established two main practical criteria. First, the propagation loss must be under 0.01 dB/m. This is to avoid excessive loss after propagation for a few L_4's, with L_4 of the order of a few meters at the targeted pulse durations for most of the considered MOF designs. Second, to limit fabrication challenges, the contrast between D and d must be as moderate as possible. Based on these two criteria we selected the MOF design with the following parameters: Λ = 1.92 μm, D = 1.027 μm, and d = 0.578 μm. As shown in Fig. 2, this design represents a good compromise between loss and fabrication feasibility.

The calculated GVD, TOD, and FOD as a function of wavelength for this particular MOF design are shown in Figs. 4(a)- 4(c). The relationship of β_2 with wavelength approximately matches the expression introduced in Eq. (1), which supports the validity of our analysis. In this case $\beta_{20} = 1.4 \times 10^{-2}$ ps^2/km, $\beta_{30} \approx 0$, and $\beta_{40} = -1.18 \times 10^{-4}$ ps^4/km at the center wavelength λ_0 = 1550 nm, or equivalently at the center angular frequency $\omega_0 = 1.22 \times 10^{15}$ rad/s.

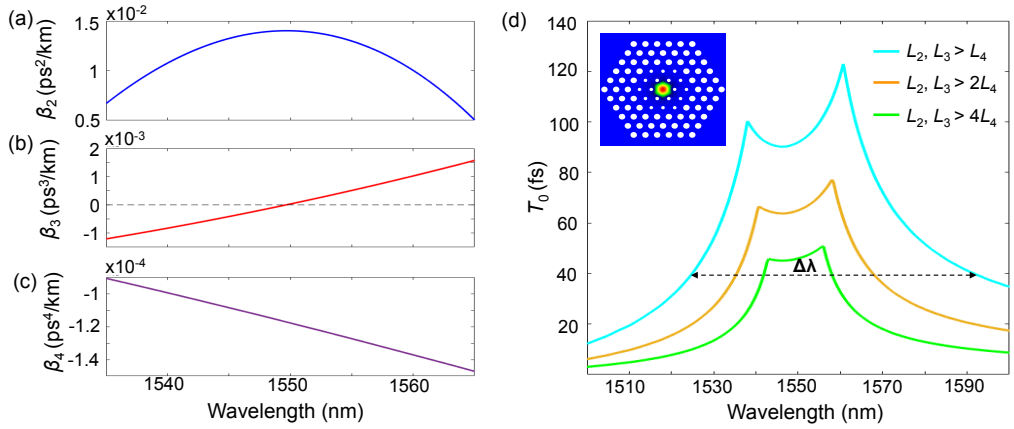

Fig. 4. Dispersion values and relation between dispersion lengths for specific microstructured optical fiber design. (a)-(c) GVD, TOD and FOD as a function of wavelength; (d) Pulse durations as a function of wavelength for which L_2>L_4 and L_3>L_4 (cyan), L_2>$2L_4$ and L_3>$2L_4$ (orange),L_2>$4L_4$ and L_3>$4L_4$ (green).Inset: MOF cross-section and mode profile.

Using the dispersion curves in Figs. 4(a)- 4(c), we calculated the characteristic dispersion lengths for a range of pulse durations realistically obtainable with a commercial femtosecond laser T_0 = [10-140] fs. Subsequently, we found the wavelength regions in which FOD is dominant over GVD and TOD by looking for the boundaries set in Eqs. (3). Figure 4(d) shows the location of these boundaries for $\alpha_2 = \alpha_3 = 1$ (cyan), $\alpha_2 = \alpha_3 = 2$ (orange), and $\alpha_2 = \alpha_3 = 4$ (green). Therefore the area under the cyan curve represents moderate FOD dominance whereas the areas under the orange and green curves represent increasing levels of FOD dominance. For a pulse duration T_0 = 40 fs at 1550 nm, for instance, the width of the moderate FOD dominant region is $\Delta\lambda$ = 67 nm. This is sufficient to loosely accommodate the whole bandwidth of a PQS pulse of that duration that, assuming an approximately Gaussian PQS shape [1] with time × bandwidth ≈ 0.44, is 53 nm. Further, a significant part of the pulse bandwidth fits within the areas of strongly dominant FOD. This is also consistent with the requirement established in Eq. (4), which at this pulse duration is satisfied for every α_2>1. Finally, we found that the available bandwidth is always determined by the second of Eqs. (3), which is always the most restrictive far from the pulse center, in accordance with the conclusion extracted from Eq. (7).

After verifying that the dispersion requirements are satisfied, we consider the nonlinear properties of the MOF. The inset in Fig. 4(d) shows the MOF cross-section and the calculated modal field profile, which yields a modal effective area $A_{\text{eff}} \approx 14.5\ \mu$m. This small effective area, around 7 times smaller than that of standard single mode fibers, ensures large nonlinearity. Specifically, given the nonlinear parameter of silica $n_2 = 2.6\times10^{-20}$ m^2/W, the expected nonlinear parameter is $\gamma \approx 7 \times 10^{-2}$ m^{-1}W^{-1}. In the context of using these fibers for the generation of high-energy ultrashort pulses, it is worth noting that the PQS energy scales linearly with the effective area and there is therefore a trade off between achieving large nonlinearities – and thus PQS formation in short fiber lengths using low input powers – and yielding high output energy. This is an inherent limitation to any soliton system, however, PQSs advantageous energy scaling guarantees that dramatically higher energies can be achieved for the same pulse duration with respect to NLS solitons.

Using the dispersion and nonlinear parameters discussed above, we simulated the propagation of 40 fs pulses at 1550 nm along $10 \times L_4$ in the MOF for different power levels by numerically solving the NLSE [1, 5]. The simulations shown in Fig. 5 include only the effects of FOD and

Optics EXPRESS

SPM for the sake of clarity. We have verified that FOD is clearly dominant over all the other orders of dispersion for 40 fs pulses ($L_4 = 0.19L_4 = 0.01L_3 = 0.5L_5$) and, whereas the results of the NLSE simulations may change slightly when including all the orders of dispersion up to β_5, the qualitative behavior does not change. First we focus our attention on the linear regime, at a peak power $P_0 = 0.3$ W. As shown in Fig. 5(a) the pulse spectrum remains unchanged after ten propagation lengths, with $L_4 = 21.7$ m. However, in the time domain, Fig. 5(b), the pulse broadens significantly due to FOD. At the output the pulse duration is 61 fs, as shown by the solid blue curve, 50% wider than the input pulse. The output phase (dashed black) exhibits a concave profile and a quartic dependence with time, as expected from linear propagation in a FOD dominant regime.

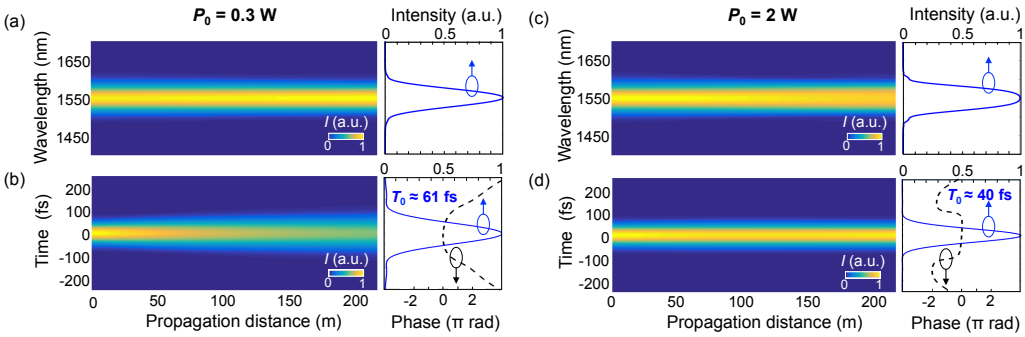

Fig. 5. Pulse propagation in microstructured optical fiber design. (a-b) Pulse propagation in the frequency and time domains respectively for a 40 fs pulse with a $P_0 = 0.3$ W. The intensity (solid blue) and the phase (dashed black) at the output are shown at the right of the propagation plot; (c-d) Similar to (a-b) for $P_0 = 2$ W, where PQSs occur.

For increasing power levels, the nonlinear Kerr effect becomes important and starts balancing the negative FOD effect. In particular at $P_0 = 2$ W, as depicted in Figs. 5(c) and 5(d), the interplay of SPM and FOD give rise to a PQS. The pulse does not broaden in the frequency or in the time domain. Further the phase (dashed black curve in 5(d)) becomes flat across the pulse duration, in a strong manifestation of soliton behavior.

5. Conclusions

The discovery of every new class of optical soliton in the past has inspired waves of new work in experiments, theory, and applications that were limited before the discovery. In a similar way, in this paper we aimed to provide the community with a rigorous understanding of the physical origin of PQSs, as well as a set of design rules for practical optical platforms suitable to observe this physical phenomenon.

We presented a formal analysis of the dispersion properties required to observe PQSs, which is general and applicable to any type of optical waveguide. Unlike NLS solitons, which can be studied in the absence of other orders of dispersion aside the GVD even in realistic platforms for sufficiently long pulses, the study of PQSs necessarily requires to consider the effect of the GVD and TOD. We analytically quantified the dominance of the quartic dispersion over the other orders of dispersion, providing the boundaries for PQS propagation in terms of pulse duration and bandwidth. This analysis furthers our understanding of this novel type of solitary wave beyond our previous experimental observations reported in [1]. Furthermore, it establishes a design toolkit that will enable the realization of PQS-supporting integrated and fiber-based platforms.

In this paper we applied these findings to the design of fiber-based platforms. In particular we provided a detailed design strategy for PQS-supporting MOFs. We provided a set of realistic

Optics EXPRESS

designs based on a common basic structure composed of 2 inner rings with small diameter and 3 outer rings with large diameter that provides a good compromise between fabrication feasibility, dispersion characteristics, and loss. We demonstrated that the designs are robust to expectable fabrication tolerances by computing the dispersion of the fibers with slightly modified parameters and demonstrating that they are still suitable for PQS propagation.

Finally, we reported NLSE simulations on a specific MOF design and verified that the interaction of the negative quartic dispersion and the Kerr nonlinearity gives rise to PQSs, even in the presence of the inherent GVD and TOD.

These results highlight the advantages of fiber platforms, which are expected to produce clean observations of PQSs and thus enable experimental evidence that leads to a formal description of important new soliton physics, such as the PQS energy scaling and higher-order soliton propagation.

Funding

Australian Research Council (ARC) Discovery Project (DP180102234); ARC Centre of Excellence CUDOS (CE110001018); University of Sydney *Professor Harry Messel Research Fellowship*; Marie Sklodowska-Curie grant of the European Union's Horizon 2020 research and innovation programme (708860).

Acknowledgments

We thank Assoc. Prof. Boris Kuhlmey for his support with the CUDOS Microstructured Optical Fiber (MOF) solver.